Journal of Superconductivity and Novel Magnetism (2022) 35:1397–1403
https://doi.org/10.1007/s10948-022-06207-7

REVIEW

Investigation of Structure and Magnetic Properties of Melt-Spun Co-Zr-(B, Al) Ribbons

Pham Thi Thanh[1,2] · Nguyen Van Duong[3] · Nguyen Mau Lam[3] · Luu Tien Hung[4] · Kieu Xuan Hau[1,2] · Nguyen Huy Ngoc[1,2] · Nguyen Hai Yen[1,2] · Nguyen Huy Dan[1,2]

Received: 12 October 2021 / Accepted: 8 March 2022 / Published online: 22 March 2022

Abstract
In this work, we investigated structure and magnetic properties of melt-spun Co-Zr-(B, Al) ribbons. The appropriate adjustment of concentration of Zr in $Co_{100-x}Zr_x$ ($x = 16$, 18, and 20) alloys is necessary to create the rhombohedral $Co_{11}Zr_2$ hard magnetic phase. The addition of B element increases the glass forming ability (GFA) of $Co_{80}Zr_{20-x}B_x$ ($x = 0$, 2, 3, and 4) alloys. The highest saturation magnetization M_s and coercivity H_c of 72.6 emu/g and 2.9 kOe are respectively obtained with B concentration of 2%. The more addition of Al and annealing process at 550 °C for 1 h facilitate $Co_{77}Zr_{20-x}Al_xB_3$ ($x = 0$, 2, 3, and 4) alloys to prevent the formation of undesired soft magnetic phases of the orthorhombic $Co_{11}Zr_2$, cubic $Co_{23}Zr_6$, and face centered cubic Co. The M_s increases from 51.5 to 62.3 emu/g with increasing Al concentration from 0 to 4%, but the H_c decreases from 4.3 to 2.8 kOe for these alloys. The obtained magnetic parameters show an application potential of the Co-Zr-based rare earth-free hard magnetic materials in practice.

Keywords Rare earth-free hard magnetic materials · Coercivity · Co-Zr alloys · Melt-spinning method

1 Introduction

The limitation of resource and high cost of rare earth elements have prompted search of new rare earth-free hard magnetic materials in recent years. Many rare earth-free hard magnetic systems have been developed such as Mn-Bi, Mn-Ga, Mn-Al, Co-Hf, Co-Zr, and Fe–Ni [1–4]. With large crystalline magnetic anisotropy ($K_1 \sim 1.1$ MJ/m^3), high Curie temperature ($T_C \sim 500$ °C), high maximum energy product ($(BH)_{max} \sim 26$ MGOe), and good corrosion resistance, Co-Zr-based magnetic materials are more and more concerned to study [5]. However, the formation of crystalline phases in the Co-Zr system is rather complicated. According to previous studies [6–8], the crystalline phases are formed in this alloy system including r-$Co_{11}Zr_2$ (rhombohedral), h-$Co_{11}Zr_2$ (hexagonal), o-$Co_{11}Zr_2$ (orthorhombic), $Co_{23}Zr_6$ (cubic), and fcc-Co (face centered cubic). Nevertheless, among these crystalline phases, only the r-$Co_{11}Zr_2$ phase creates hard magnetic properties for the Co-Zr alloys [5]. This hard magnetic phase is formed through peritectoid reaction of $L + Co_{23}Zr_6 \rightarrow Co_{11}Zr_2$ at high temperature, above 1198 K [9]. Controlling technological conditions to enhance the hard magnetic phases and suppress the soft magnetic ones for the Co-Zr alloys is really necessary. On the other hand, previous studies have shown that the obtained coercivity of the Co-Zr alloys is much smaller than the anisotropy field H_A of the r-$Co_{11}Zr_2$ phase ($H_A = 35$ kOe) [10, 11]. The addition of some elements such as Si, Cr, B, and Nb is an effective way to improve the coercivity of the Co-Zr alloys [12–16]. The synthesis method is also selected appropriately to obtain the desired microstructure, leading to enhancement the coercivity of the alloy. Arc-melting, high-energy mechanical milling, melt-spinning, and spark plasma sintering methods are commonly used to fabricate the Co-Zr materials [17–20]. Among them, the melt-spinning method is the most used one. The advantage of this method is possible to fabricate

✉ Pham Thi Thanh
thanhpt@ims.vast.ac.vn

1 Institute of Materials Science, Vietnam Academy of Science and Technology, 18 Hoang Quoc Viet, Ha Noi, Viet Nam

2 Graduate University of Science and Technology, Vietnam Academy of Science and Technology, 18 Hoang Quoc Viet, Ha Noi, Viet Nam

3 Hanoi Pedagogical University, 32 Nguyen Van Linh, Xuan Hoa, Phuc Yen, Vinh Phuc, Viet Nam

4 College of Education, Vinh University, Nghe An, 182 Le Duan, Vinh, Viet Nam

the material with large amount for practical applications and easily control the desired microstructure. The influence of the addition of metalloid elements with small atomic radius such as B and C on magnetic properties of the Co-Zr alloy was investigated. Saito and Itakura [15] indicated that the addition of small concentration of B in the $Co_{80}Zr_{20-x}B_x$ ($x = 0$–4) alloy ribbons could increase the fraction of the r-$Co_{11}Zr_2$ phase and refine the grain size, leading to increase the coercivity by 70%. Unlike B, the addition of C reduces the coercivity of the alloy. However, C increases saturation magnetization of the Co-Zr materials by the enhancement of the $Co_{23}Zr_6$ and fcc-Co soft magnetic phases [21]. The Hf, Mo, and W elements, which have large atomic radius, can also improve the coercivity of Co-Zr materials [22–25]. In the case of addition of Hf, the $Co_{82}Zr_{18-x}Hf_x$ ($x = 0$, 2, 4, and 6) ribbons show an independence of the crystalline magnetic anisotropy on the concentration of the addition element. The reduction in the ratio of the fcc-Co soft and the r-$Co_{11}Zr_2$ hard magnetic phase is responsible for linear increase of the coercivity from 2.4 to 3.3 kOe with increasing Hf concentration from 0 to 6% [22]. According to Zhang et al. [23], the coercivity reaches the maximum value of 4.1 kOe for $Zr_{18}Co_{77}Mo_5$ alloy ribbons. After adding W, the coercivity increased from 2.2 kOe for un-added alloy to 4.35 kOe for 5% W-added alloy [25]. All above mentioned studies showed an increase of coercivity, but a decrease of the saturation magnetization with increasing concentration of the addition elements. For the $Co_{82-x}Zr_{18}Cu_x$ ($x = 0$–3) alloy ribbons, increasing Cu concentration leads to an increase of the fraction of the o-$Co_{11}Zr_2$ phase. As a result, the coercivity decreases monotonically from 2.2 to 1.5 kOe, while the saturation magnetization strongly increases from 56 to 101 emu/g [14]. To further improve the coercivity, the influence of multiple elements in Zr-Co system was also studied by other researchers [11, 12, 16, 17]. The combined enhancement of the anisotropic field of the r-$Co_{11}Zr_2$ phase by Si and promoting the formation of hard magnetic phase by B resulted in improving both the coercivity and the saturation magnetization. The obtained H_c and M_s values of the $Co_{80}Zr_{17}Si_1B_2$ ribbons reached 4.5 kOe and 64 emu/g, respectively [27]. Jin et al. [16] added Mo and B together, leading to an enhancement of H_c to 5.4 kOe for the $Co_{81.5}Zr_{16}Mo_{1.5}B_1$ alloy (up to 91% compared to the $Co_{82.5}Zr_{16}Mo_{1.5}$ sample). Zhou et al. [11] obtained high H_c of 7.7 kOe on Co-Zr-Cr-Si-B alloy by the inhabitable formation of fcc-Co soft magnetic phase. On the other hand, corrosion resistance of the alloy is also significantly improved compared to rare earth magnets. Thus, the addition of elements is an effective way in improving the magnetic properties of the Co-Zr alloy. However, the influential rules of additional elements, especially the simultaneous influence of multi-additions on structure and magnetic properties of the Co-Zr alloys system, are still unclear and need to be studied further. In this work, we investigated the influence of B and Al on structure and magnetic properties of the Co-Zr alloys prepared by melt-spinning method.

2 Experiment

Alloy samples were prepared from elements of Co, Zr, B, and Al with high purity. The samples were weighed according to the desired nominal compositions and then arc-melted several times to ensure their homogeneity. Alloy ribbons with width and thickness of about 2 mm and 30 µm, respectively, were prepared by using melt-spinning method with single wheel rotating at a surface velocity of 40 m/s. Some ribbons were then annealed to further enhance their magnetic properties. In order to avoid oxidation of the samples, all the processes of arc-melting, melt-spinning, and annealing were performed under Ar atmosphere. X-ray diffraction (XRD) method on an Equinox 5000—Thermo Scientific instrument with Cu-K_α radiation source ($\lambda = 1.5406$ Å) was used to analyze structure of the samples. Magnetic properties of the alloy ribbons were investigated on a pulsed field magnetometer (PFM) with maximum magnetic field of 90 kOe.

3 Results and Discussion

Firstly, we investigated structure and magnetic properties of binary Co-Zr alloy ribbons with Zr concentrations in the range of 16 to 20%. XRD patterns of the $Co_{100-x}Zr_x$ ($x = 16$, 18, and 20) ribbons are shown in Fig. 1. The obtained results show that the diffraction peaks correspond to the r-$Co_{11}Zr_2$, o-$Co_{11}Zr_2$, $Co_{23}Zr_6$, and fcc-Co phases. The diffraction peaks with high intensity are mainly

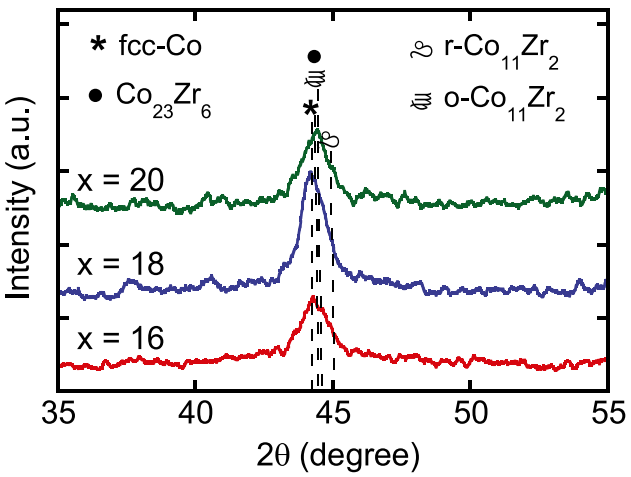

Fig. 1 XRD patterns of the $Co_{100-x}Zr_x$ ($x = 16$, 18, and 20) ribbons

concentrated in the 2θ angle from 40 to 45°. However, it is difficult to observe the individual phases because the diffraction peaks in the Co-Zr alloys overlap each other. On the other hand, the estimation of relative proportion of the crystalline phases in the alloy ribbons is also difficult. Based on the standard card data, we determined the r-$Co_{11}Zr_2$ (JCPDS No. 00–059-0161), o-$Co_{11}Zr_2$ (JCPDS No. 00–059-0162), fcc-$Co_{23}Zr_6$ (JCPDS No. 01–079-3504), and fcc-Co (JCPDS No. 00–015-0806) phases at different 2θ angles of 44.67°, 44.48°, 44.41°, and 44.22°, respectively. We can observe that the formation of crystalline phases depends on the Zr concentration. The structure of the 16% Zr and 18% Zr alloys indicates a dominance of the fcc-Co phase. However, the diffraction peaks of the sample with the Zr concentration of 18% are sharper than those of the 16% Zr sample. The diffraction peaks of the other phases have low intensity so it is difficult to observe them on the XRD patterns. With the Zr concentration of 20%, the fraction of the fcc-Co phase gradually decreases and there is a shift of the diffraction peak toward the large 2θ angle corresponding to the increase in the fraction of the o-$Co_{11}Zr_2$ and $Co_{23}Zr_6$ phases. Notably, the intensity of diffraction peak at the position corresponding to the r-$Co_{11}Zr_2$ hard magnetic phase tends to increase. Other studies showed that the crystalline phases are formed in Co-Zr alloys including $Co_{11}Zr_2$, $Co_{23}Zr_6$, and Co phases [7, 10]. However, the adjustment for appropriate Zr concentration can prevent the formation of phases which are not in favor of hard magnetic properties of the alloy. Gabay et al. [7] indicated that, with low Zr concentrations below 16%, the fcc-Co phase is dominant. The alloy is nearly single r-$Co_{11}Zr_2$ phase with 16.4% Zr. When the Zr concentration is greater than 20%, a large amount of $Co_{23}Zr_6$ phase is formed.

Figure 2 shows hysteresis loops of the $Co_{100-x}Zr_x$ (x = 16, 18, and 20) ribbons. We can see that, the concentration of Zr clearly influences on the coercivity H_c and saturation magnetization M_s of the samples (the inset of Fig. 2). The coercivity increases from 1 to 1.9 kOe when the concentration of Zr increases from 16 to 20%. The obtained results are in good agreement with the structure of the alloy ribbons analyzed on their XRD patterns in Fig. 1. With low Zr concentration (16% and 18%), fraction of the soft magnetic phases is large, leading to low coercivity. Meanwhile, the contribution of the r-$Co_{11}Zr_2$ hard magnetic phase increases in the sample with higher Zr concentration (20%), resulted in an improvement of the coercivity. However, the phase r-$Co_{11}Zr_2$ is moderately developed in the given condition, resulting in low intensity diffraction peak and low H_c. The variation of coercivity according to Zr concentration is similar to the results obtained by Saito [33]. The coercivity of $Co_{80}Zr_{20}$ alloy ribbons reaches a maximum value of 2.3 kOe. Unlike coercivity, the saturation magnetization M_s decreases from

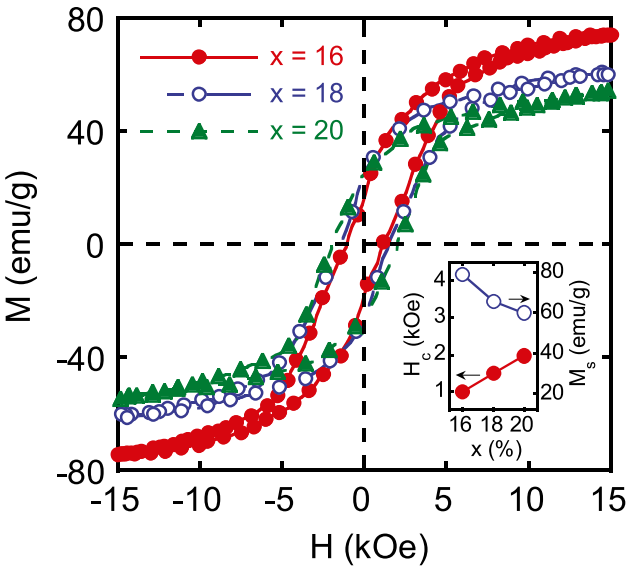

Fig. 2 Hysteresis loops of the $Co_{100-x}Zr_x$ (x = 16, 18, and 20) ribbons. The inset is the dependence of saturation magnetization M_s and coercivity H_c on Zr concentration

79 to 60 emu/g when the concentration of Zr increases from 16 to 20%. This decrease is explained by the increase in the concentration of the Zr non-ferromagnetic atoms in the alloy.

Based on the above results, we realize that the coercivity of the binary Co-Zr alloy ribbons obtained low value of 1.9 kOe. This value cannot meet the application requirements in practice. Therefore, the addition of elements is chosen to further enhance the magnetic properties of the material. Initially, the influence of B on structure and magnetic properties of the $Co_{80}Zr_{20-x}B_x$ (x = 0, 2, 3, and 4) alloy ribbons was investigated. The structure of this alloy ribbons is examined through the XRD patterns (Fig. 3). The o-$Co_{11}Zr_2$, r-$Co_{11}Zr_2$, $Co_{23}Zr_6$, and fcc-Co phases were found in the

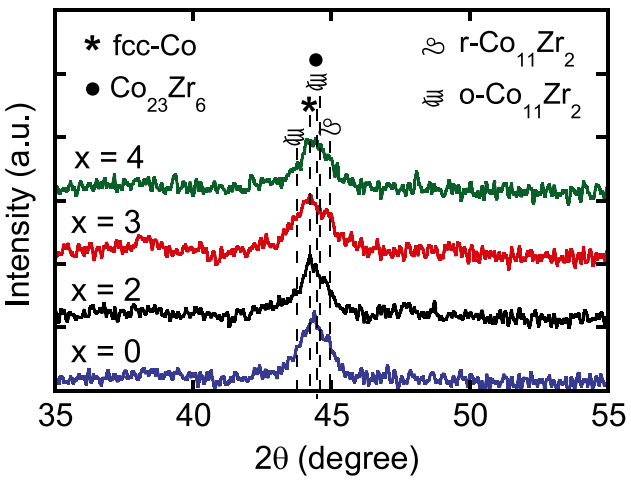

Fig. 3 XRD patterns of the $Co_{80}Zr_{20-x}B_x$ (x = 0, 2, 3, and 4) ribbons

B-added alloys. The diffraction peaks become lower and wider when the concentration of B increases from 0 to 4%. This proves that the glass forming ability (GFA) of the alloy is increased by the addition of B.

The different concentrations of B influence on the structure, leading to the change of the magnetic properties of the $Co_{80}Zr_{20-x}B_x$ ($x=0$, 2, 3, and 4) ribbons as presented in Fig. 4. We can see that, the shape and squareness of the hysteresis loops are significantly improved in comparison to those of the B-free alloy. In order to clearly observe, the dependence of coercivity H_c and saturation magnetization M_s on B concentration is shown in the inset of Fig. 4. The H_c increases from 1.9 to 3 kOe with increasing the B concentration from 0 to 2%. Then it decreases slightly as the B concentration is increased further to 3% and 4%. The highest coercivity obtained with B concentration of 2% is in good agreement with the structural results from the XRD patterns in Fig. 3. Small fraction of the r-$Co_{11}Zr_2$ hard magnetic phase and the formation of other soft magnetic phases lead to low coercivity of the alloy. As for the saturation magnetization, its variation on the B concentrations is different from that of the coercivity. The saturation magnetization of the ribbons is greatly increased from 59.5 to 72.6 emu/g when the concentration of B increases from 0 to 2%. Then, it slowly increases and reaches values of 74.2 emu/g and 75.5 emu/g at 3% B and 4% B, respectively. Thus, the optimal B concentration for hard magnetic property is 2%. Chang et al. [27] indicated that, B is an element that strongly increases the glass forming ability or amorphous state of the alloy. According to the general principle, the GFA is increased when the alloy has many components with large difference of the atomic sizes. In this case, B has much smaller atomic size than that of the elements. On the other hand, the melting point is reduced by the increasing the B concentration, leading to the formation of the amorphous structure of the melt-spun ribbons. Therefore, the higher concentration of B prevents the formation of crystalline phases in general and the r-$Co_{11}Zr_2$ phase in particular, resulting in the reduction of the coercivity of the alloy. The study of Saito and Itakura [15] also showed that, the addition of B in the $Co_{80}Zr_{20}$ alloy with concentration of 2% was effective in creating uniform, refine particles and the enhancement of the formation of the r-$Co_{11}Zr_2$ hard magnetic phase, leading to high coercivity.

As mentioned in "Sect. 1," in order to create the high coercivity, in addition to the large magnetic anisotropy of the hard magnetic phase, the materials need to have the desired microstructure. Some studies have shown that the addition of the non-ferromagnetic elements such as Cu and Al to the Co-Zr alloys can increase the fraction of the desired phase and improve the microstructure such as refining grains, uniforming grain boundaries. For example, the addition of Cu in the $Co_{80-x}Zr_{18}Cu_xB_2$ ($x=0$, 1, 2, 3, and 4) alloy ribbons changed strongly relative ratio of the o-$Co_{11}Zr_2$ and r-$Co_{11}Zr_2$ phases, to obtain coercivity of 4.7 kOe [26]. Al was also selected as an adding element in the study of Chang et al. for the $Co_{80}Zr_{17}A_lB_2$ alloy [27]. Nevertheless, the coercivity of $Co_{80}Zr_{17}A_lB_2$ alloy, which only reaches 3.5 kOe, is smaller than that of the Al-free alloy ($H_c \sim 4.4$ kOe). The decrease of coercivity is due the reduction of magnetocrystalline anisotropy field of r-$Co_{11}Zr_2$ phase. However, this research team only investigated the alloy with Al concentration of 1%. Therefore, in this work, we investigated with Al concentrations in a range of 0–4% and in combined with an annealing process. The structure of the $Co_{77}Zr_{20-x}Al_xB_3$ ($x=0$, 2, 3, and 4) alloy ribbons is shown

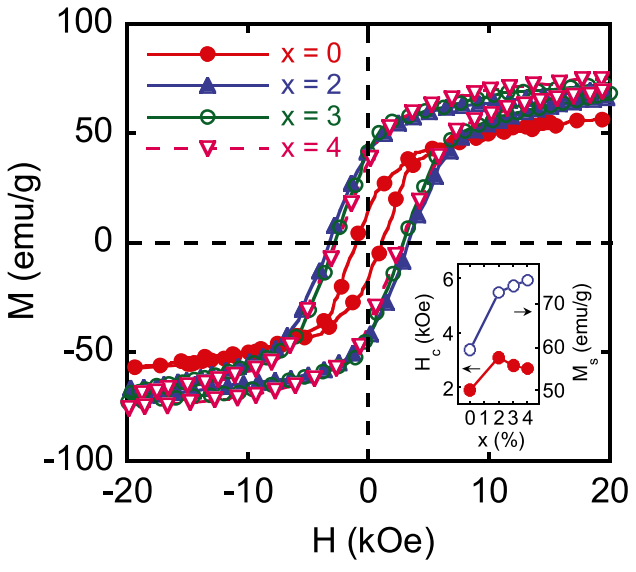

Fig. 4 Hysteresis loops of the $Co_{80}Zr_{20-x}B_x$ ($x=0$, 2, 3, and 4) ribbons. The inset is the dependence of saturation magnetization M_s and coercivity H_c on B concentration

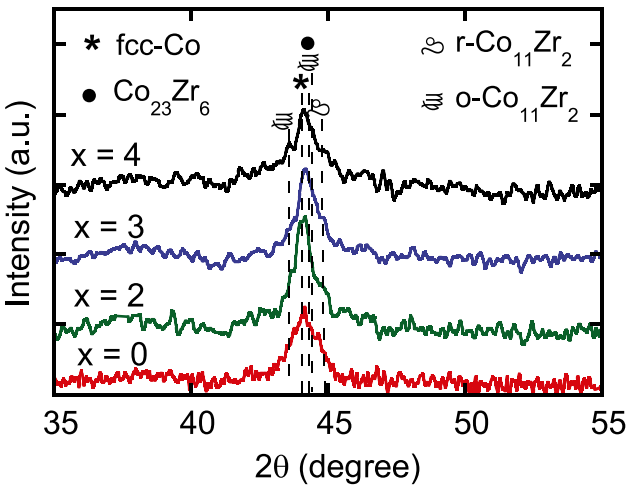

Fig. 5 XRD patterns of the $Co_{77}Zr_{20-x}Al_xB_3$ ($x=0$, 2, 3, and 4) ribbons

in Fig. 5. We can see that, the crystallization of the alloy is significantly improved. The expansion of diffraction peak of the alloy without containing Al shows that the amorphous phase is dominant. When Al is added to the alloy, the width of diffraction peaks is narrowed and the intensity of them is increased. It is found that the r-$Co_{11}Zr_2$ hard magnetic phase is formed with weak intensity along with the o-$Co_{11}Zr_2$, $Co_{23}Zr_6$, and fcc-Co phases in the ribbon with 2% Al and then gradually disappeared in the samples with 3% and 4% Al. Meanwhile, the diffraction peak corresponding to the o-$Co_{11}Zr_2$ phase is enhanced when the Al concentration of 4%. Thus, the addition of Al can improve the crystallization of the alloy ribbons. However, it is important to choose the appropriate concentration to create the desired microstructure in favor of hard magnetic property of the alloy.

The influence of the structure on the magnetic properties of the alloy ribbons is presented in the hysteresis loops in Fig. 6. We can realize that the squareness of the hysteresis loops of the alloys is significantly improved by the addition of Al. Besides, the Al addition influences on the saturation magnetization and coercivity of the alloy (the inset in Fig. 6). The M_s increases from 51.5 to 62.3 emu/g with the increasing of the Al concentration from 0 to 4%. The saturation magnetization insignificantly increases at 3% and 4% of Al and reaches 61.7 emu/g and 62.3 emu/g, respectively. Meanwhile, the variation of coercivity on the Al concentrations is different from that of the saturation magnetization. The coercivity of the alloys decreases monotonically when Al element is added. The H_c slightly decreases from 3.9 to 3.8 kOe as the Al concentration increases from 0 to 2%. After that, the coercivity fast declines to 2.3 kOe and 2.1 kOe, respectively, as the Al concentration is further increased up to 3% and 4%. The strong decrease of the coercivity with high Al concentrations of 3% and 4% probably is due to the large fraction of the soft magnetic phases in the alloy as proved by the structural analyzes on the XRD patterns (Fig. 5). Thus, the adjustment of Al concentration strongly influences on the magnetic properties of the alloy.

In order to further enhance the coercivity, the $Co_{77}Zr_{20-x}Al_xB_3$ ($x=0$, 2, 3, and 4) alloy ribbons were annealed. Selecting an appropriate annealing regime may prevent the formation of undesired phases. According to a recent research by Christopher et al. [13], by annealing at temperature of 550 °C for 1 h, the r-$Co_{11}Zr_2$ diffraction peaks with high intensity were observed in $Zr_2Co_{9.5}Fe_{1.5}B$ alloy ribbons. Another research [28] showed that, at high annealing temperature (700 °C), the metastable $Co_{11}Zr_2$ phase can decompose into $Co_{23}Zr_6$ and Co according to the $Co_{11}Zr_2 \rightarrow Co_{23}Zr_6 + Co$ reaction. The increasing soft magnetic phases influences on the magnetic reversal nucleation sites, leading to decrease the coercivity. Hou et al. [28] obtained the coercivity of 7 kOe in the rapidly quenched $Co_{77}Zr_{18}Cr_3B_2$ alloy after annealing at 550 °C. The significant enhancement of the coercivity of this annealing temperature can be explained by the random anisotropy model [29]. According to this model, when the crystalline particle size is approximately equal to the exchange interaction length, the highest coercivity is obtained. In case the particle size is smaller or larger than exchange interaction length, the random magnetic anisotropy decreases, leading to low H_c

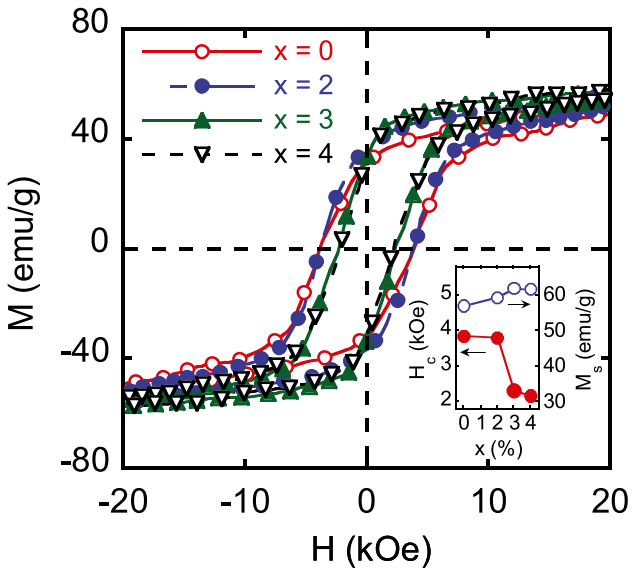

Fig. 6 Hysteresis loops of the $Co_{77}Zr_{20-x}Al_xB_3$ ($x=0$, 2, 3, and 4) ribbons. The inset is the dependence of saturation magnetization M_s and coercivity H_c on Al concentration

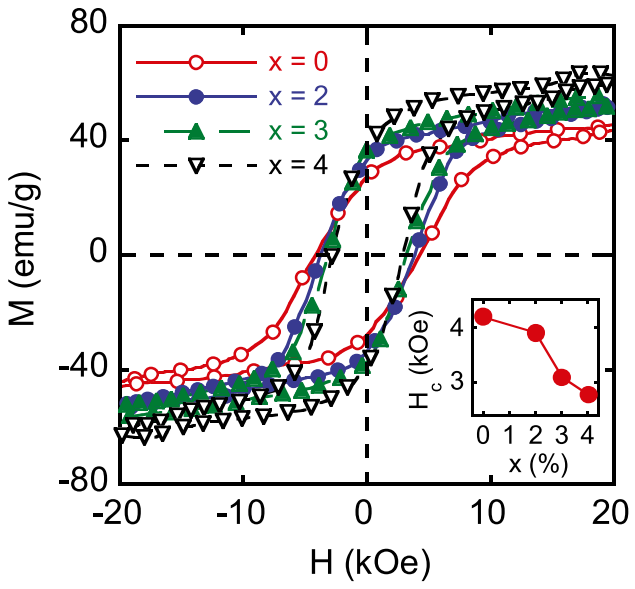

Fig. 7 Hysteresis loops of $Co_{77}Zr_{20-x}Al_xB_3$ ($x=0$, 2, 3, and 4) ribbons annealed at 550 °C for 1 h. The inset is the dependence of coercivity H_c on Al concentration

Table 1 Comparison of the magnetic properties of alloy ribbons in this work and the Co-Zr-based alloys reported previously

Nominal composition	T_a (°C)	t_a (min)	M_s (emu/g)	H_c (kOe)	Reference
$Co_{80}Zr_{20}$	–	–	65.7	1.9	This work
$Co_{80}Zr_{18}B_2$	–	–	72.6	3	This work
$Co_{77}Zr_{18}Al_2B_3$	–	–	57.3	3.8	This work
$Co_{77}Zr_{18}Al_2B_3$	550	60	57.3	4.2	This work
$Co_{82}Zr_{18}$	–	–	79.6	3.1	[30]
$Co_{80}Zr_{18}Fe_2$	–	–	79.6	2.4	[30]
$Co_{80}Zr_{18}B_2$	600	60	–	4	[15]
$Co_{82}Zr_{18}$	–	–	56	2.2	[14]
$Co_{81}Zr_{18}Cu_1$	–	–	50	1.9	[14]
$Co_{77}Zr_{18}Mo_5$	–	–	19	4.1	[22]
$Co_{77}Zr_{18}Mo_5$	650	30	–	2.5	[22]
$Co_{82}Zr_{12}Hf_6$	–	–	64	3.3	[24]
$Co_{77}Zr_{18}W_5$	–	–	–	4.3	[25]
$Co_{77}Zr_{18}W_5$	650	20	–	3.1	[25]
$Co_{80}Zr_{18}C_2$	600	60	60	1.9	[21]
$Co_{82}Zr_{15}V_3$	–	–	49	3	[32]
$Co_{82}Zr_{15}V_3$	560	20	49	3.7	[32]
$Co_{80}Zr_{17}Al_1B_2$	–	–	63	3.5	[27]
$Zr_2Co_{9.5}Fe_{1.5}B$	550	60	89.3	1.6	[13]
$Co_{78}Zr_{18}Cu_4B_2$	–	–	61	3	[26]
$Co_{78}Zr_{18}Cu_4B_2$	650	30	60	5.3	[26]
$Co_{80}Zr_{15}Ti_3B_2$	–	–	50	1.5	[31]
$Co_{80}Zr_{15}Ti_3B_2$	650	2	50	4.3	[31]
$Co_{81.5}Zr_{16}Mo_{1.5}B_1$	–	–	–	5.4	[16]
$Co_{78}Zr_{16}Si_3B_3$	–	–	61	2.9	[12]
$Zr_{16}Co_{75}Nb_3Si_3B_3$	–	–	42	4.8	[12]
$Co_{74}Zr_{16}Cr_4Si_3B_3$	–	–	25.5	7.7	[11]

value. Thus, with annealing at 550 °C, the alloy obtained optimal particle size, resulted in the high coercivity. In this work, the $Co_{77}Zr_{20-x}Al_xB_3$ ($x = 0$, 2, 3, and 4) alloy ribbons were annealed at 550 °C for 1 h. After that, the samples are fast cooled from annealing temperature to avoid the formation of the intermediate phases, which are not conducive to the hard magnetic properties of the samples. From the hysteresis loops in Fig. 7, we determined the dependence of the coercivity on the Al concentration, which is presented in the inset of the figure. It is found that the annealing process improves the coercivity of all the samples. The change of H_c with Al concentration is similar to that of the as-quenched ribbons. The coercivity decreases slightly from 4.3 to 4.2 kOe when the Al concentration increases from 0 to 2%. Continuing to increase the Al concentration to 3% and 4%, the H_c decreases to 3.1 kOe and 2.8 kOe, respectively.

A comparison of the magnetic properties of alloy ribbons in this work and the added Co-Zr alloys reported previously is shown in Table 1. We can realize that, by addition of different elements to the alloy, the optimal magnetic parameters are varied. Our obtained values of the saturation magnetization M_s and coercivity H_c are moderate in comparison with those of the similar composition of other research groups.

4 Conclusion

Structure and magnetic properties of the melt-spun Co-Zr-(B, Al) ribbons were investigated. The formation of r-$Co_{11}Zr_2$, o-$Co_{11}Zr_2$, $Co_{23}Zr_6$, and fcc-Co crystalline phases in the alloys strongly depends on composition and synthesis conditions, resulting in the change of their hard magnetic behavior. The addition of B element increases the glass forming ability for the alloy. The coercivity is enhanced from 1.9 kOe for the binary $Co_{80}Zr_{20}$ alloy ribbons to 3 kOe for the ternary $Co_{80}Zr_{18}B_2$ ones. As for the quaternary $Co_{77}Zr_{18}Al_2B_3$ alloy ribbons, their coercivity can reach 4.2 kOe after annealing at 550 °C for 1 h. The optimizing technological conditions could enhance the magnetic parameters to meet requirements for applications of the Co-Zr-based rare earth-free hard magnetic materials.

Acknowledgements A part of the work was done in the Key Laboratory for Electronic Materials and Devices, Institute of Materials Science, Viet Nam.

Funding This research is funded by the National Foundation for Science and Technology Development (NAFOSTED) of Viet Nam under grant number of 103.02–2018.339.

References

1. Volegov, A.S., Muller, K.H., Bittner, F., Mix, T., Neznakhin, D.S., Volegova, E.A., Schultz, L., Woodcock, T.G., Nenkov, K.: Magnetic viscosity of $L1_0$ structured Mn-Ga and Mn-Al alloys. J. Magn. Magn. Mater. **441**, 750–756 (2017)
2. Chang, H.W., Liao, M.C., Shih, C.W., Chang, W.C., Yang, C.C., Hsiao, C.H., Ouyang, H.: Hard magnetic property enhancement of Co_7Hf-based ribbons by boron doping. Appl. Phys. Lett. **105**, 192404 (2014)
3. Balamurugan, B., Das, B., Zhang, W.Y., Skomski, R., Sellmyer, D.J.: Hf-Co and Zr-Co alloys for rare-earth-free permanent magnets. J. Phys. Condens. Matter. **26**, 064204 (2014)
4. Goto, S., Kura, H., Watanabe, E., Hayashi, Y., Yanagihara, H., Shimada, Y., Mizuguchi, M., Takanashi, K., Kita, E.: Synthesis of single-phase $L1_0$-FeNi magnet powder by nitrogen insertion and topotactic extraction. Sci. Rep. **7**, 13216 (2017)
5. Cui, J., Kramer, M., Zhou, L., Liu, F., Gabay, A., Hadjipanayis, G., Balasubramanian, B., Sellmyer, D.: Current progress and future challenges in rare-earth-free permanent magnets. Acta Mater. **158**, 118–137 (2018)
6. Pechin, W.H., Williams, D.E., Larsen, W.L.: The zirconium-cobalt alloy system. Trans. ASM **57**, 464–473 (1964)
7. Gabay, A.M., Zhang, Y., Hadjipanayis, G.C.: Cobalt-rich magnetic phases in Zr-Co alloys. J. Magn. Magn. Mater. **236**, 37–41 (2001)
8. Ivanova, G.V., Shchegoleva, N.N., Gabay, A.M.: Crystal structure of Zr_2Co_{11} hard magnetic compound. J. Alloy. Compd. **432**, 135–141 (2007)
9. Zhao, X., Nguyen, M.C., Zhang, W.Y., Wang, C.Z., Kramer, M.J., David, J.S., Li, X.Z.: Exploring the structural complexity of intermetallic compounds by an adaptive genetic algorithm. Phys. Rev. Lett. **112**, 045502 (2014)
10. Saito, T.: Microstructures and magnetic properties of Co-Zr system alloys. Mater. Trans. **44**, 1713–1716 (2003)
11. Zhou, X., Zhang, J. Liao, X., He, J., Li, K., Liu, Z.: Beneficial effects of Cr addition on the nanocrystalline Si and B modified CoZr permanent magnetic alloys. J. Magn. Magn. Mater. **501**, 166483 (2020)
12. Rama Rao, N.V., Nagendra, M.V., Sridhara Rao, D.V., Aravindha Babu, D., Chary, V.R., Mathur, R.P.: Structural and magnetic properties of Nb substituted Zr-Co-Si-B nanocrystalline ribbons. Intermetallics **101**, 8–12 (2018)
13. Christopher, N., Anand, K., Singh, N.: Enhancement of hard magnetic properties in rapidly quenched Zr–Co–Fe–B ribbons through vacuum annealing. Solid State Commun. **323**, 114118 (2021)
14. Imtyaz, M.D., Rama Rao, N.V., Aravindha Babu, D., Ramesh Chandra, B., Pandian, S.: Effect of Cu substitution on structural and hard magnetic properties of rapidly solidified $Zr_{18}Co_{82-x}Cu_x$ melt spun ribbons. J. Alloy. Compd. **699**, 657–661 (2017)
15. Saito, T., Itakura, M.: Microstructures of Co-Zr-B alloys produced by melt-spinning technique. J. Alloys Compd. **572**, 124–128 (2013)
16. Jin, Y., Zhang, W., Kharel, P.R., Valloppilly, S.R., Skomski, R., Sellmyer, D.J.: Effect of boron doping on nanostructure and magnetism of rapidly quenched Zr_2Co_{11}-based alloys. AIP Advan. **6**, 056002 (2016)
17. Rama Rao, N.V., Nagendra, M.V., Priyanka, N., Aravindha Babu, D., Chary, V.R., Mathur, R.P.: Structural and magnetic properties of nanocrystalline Zr-Co-Nb-Si-B rare earth free permanent magnets fabricated by spark plasma sintering. J. Magn. Magn. Mater. **476**, 329–333 (2019)
18. Neelima, B., Rao, N.R., Chary, V.R., Pandian, S.: Influence of mechanical milling on structure, particle size, morphology and magnetic properties of rare earth free permanent magnetic Zr_2Co_{11} alloy. J. Alloys Compd. **661**, 72–76 (2016)
19. Mehrdad, F.P., Ali, K., Valiollah, D.: Effect of milling and adding yttrium on sorption characteristics of Zr-Co based nanostructure chemical getter. J. Alloys Compd. **846**, 155329 (2020)
20. Bhardwaj, V., Satyendra, P.P., Rama Rao, N.V., Ratnamala, C.: Structural and magnetic properties of [110] oriented Co_5Zr hard magnetic thin films. Mater. Lett. **260**, 126869 (2020)
21. Saito, T., Kamagata, Y., Wang, W.Q.: The origin of high-saturation magnetization in Co-Zr-C melt-spun ribbons. IEEE Trans. Magn. **41**, 3787–3789 (2005)
22. Omari, A.A., Zhang, W.Y., Yue, L., Skomski, R., Shield, J.E., Li, X.Z., Sellmyer, D.J.: Hf doping effect on hard magnetism of nanocrystalline $Zr_{18-x}Hf_xCo_{82}$ ribbons. IEEE Trans. Magn. **49**, 3394–3397 (2013)
23. Zhang, J.B., Sun, Q.W., Wang, W.Q., Su, F.: Effects of Mo additive on structure and magnetic properties of $Co_{82}Zr_{18}$ alloy. J. Alloy. Compd. **474**, 48–51 (2009)
24. Zhang, W.S., Valloppilly, R., Li, X., Skomski, R., Shield, J.E., Sellmyer, D.J.: Coercivity enhancement in Zr_2Co_{11}-based nanocrystalline materials due to Mo addition. IEEE Trans. Magn. **48**, 3603–3605 (2012)
25. Xu, S., Xu, D., Hou, Z., Zhang, J., Su, F., Sun, L., Wang, W.: The structure and magnetic properties of $Co_{77}Zr_{18}W_5$ melt-spun ribbons. World J. Conden. Matter Phys. **2**, 197–201 (2012)
26. Lee, G., Kim, J.: Effects of Cu addition on magnetic properties and microstructures of annealed Zr–Co–Cu–B ribbons. IEEE Trans. Magn. **53**, 2101104 (2017)
27. Chang, H.W., Tsai, C.F., Hsieh, C.C., Shih, C.W., Chang, W.C., Shaw, C.C.: Magnetic properties enhancement of melt spun CoZrB ribbons by elemental substitutions. J. Magn. Magn. Mater. **346**, 74–77 (2013)
28. Hou, Z., Li, H., Wang, W.: The origin of coercivity enhancement in the $Co_{77}Zr_{18}Cr_3B_2$ magnet. J. Alloy. Compd. **593**, 1–6 (2014)
29. Herzer, G.: Grain structure and magnetism of nanocrystalline ferromagnets. IEEE Trans. Magn. **25**, 3327–3329 (1989)
30. Zhou, X., Liu, Z., Yu, H., Zhang, H., Zhang, G.: Optimization of rapidly quenched Co–Zr and (Co,Fe)–Zr alloys for rare earth free permanent magnets. Phys. B: Condens. Matter. **599**, 412549 (2020)
31. Hou, Z., Xu, S., Zhang, J., Wu, C., Liu, D., Su, F., Wang, W.: High performance $Co_{80}Zr_{15}Ti_3B_2$ melt-spun ribbons. JAC. **555**, 28–32 (2013)
32. Hou, Z., Su, F., Xu, S., Zhang, J., Wu, C., Liu, D., Wei, B., Wang, W.: Magnetic properties, phase evolution, and microstructure of the Co–Zr–V ribbons. J. Magn. Magn. Mater. **346**, 124–129 (2013)
33. Saito, T.: Microstructures and magnetic properties of Co–Zr system alloys. Mater. Trans. **44**, 1713–1716 (2003)